applied sciences

MDPI

Article

Atrazine-Induced Hepato-Renal Toxicity in Adult Male *Xenopus laevis* Frogs

Lynette Sena [1], Jaclyn Asouzu Johnson [1,*], Pilani Nkomozepi [2] and Ejikeme Felix Mbajiorgu [1]

[1] School of Anatomical Sciences, University of the Witwatersrand, Johannesburg 2193, South Africa; rufaro.sena@gmail.com (L.S.); ejikeme.mbajiorgu@wits.ac.za (E.F.M.)
[2] Department of Human Anatomy and Physiology, University of Johannesburg, Johannesburg 2006, South Africa; pilanin@uj.ac.za
* Correspondence: jaclyn.johnson@wits.ac.za

Abstract: Atrazine (ATZ) is an herbicide commonly detected in groundwater. Several studies have focused on its immunological and endocrine effects on adult *Xenopus laevis* species. However, we investigated the impact of atrazine on the renal and hepatic biochemistry and histomorphology in adult male frogs. Forty adult male frogs were allocated to four treatment groups (control, one ATZ (0.01 µg/L), two ATZ (200 µg/L) and three ATZ (500 µg/L), 10 animals per group, for 90 days. Alanine aminotransferase (ALT) and creatinine levels increased significantly ($p < 0.05$) in the 200 and 500 µg/L groups but malondialdehyde only in the 500 µg/L group ($p < 0.05$). Histopathological observations of derangement, hypertrophy, vascular congestion and dilation, infiltration of inflammatory cells incursion, apoptosis and hepatocytes cell death were observed with atrazine exposure, mostly in the 500 µg/L group. Additionally, histochemical labelling of caspase-3 in the sinusoidal endothelium was observed in all the treated groups, indicating vascular compromise. Evaluation of renal histopathology revealed degradation and atrophy of the glomerulus, vacuolization, thick loop of Henle tubule epithelial cells devolution and dilation of the tubular lumen. Furthermore, expression of caspase-3 indicates glomerular and tubular apoptosis in atrazine-exposed animals. These findings infer that environmentally relevant atrazine doses (low or high) could induce hepatotoxicity and nephrotoxicity in adult male *Xenopus laevis* frogs and potentially related aquatic organisms.

Keywords: atrazine; hepatorenal; pathology; toxicosis; biomarkers; adult *Xenopus laevis*

Citation: Sena, L.; Asouzu Johnson, J.; Nkomozepi, P.; Mbajiorgu, E.F. Atrazine-Induced Hepato-Renal Toxicity in Adult Male *Xenopus laevis* Frogs. *Appl. Sci.* **2021**, *11*, 11776. https://doi.org/10.3390/app112411776

Academic Editors: Panagiotis Berillis and Božidar Rašković

Received: 30 October 2021
Accepted: 6 December 2021
Published: 11 December 2021

1. Introduction

Atrazine (ATZ) as (2-chloro-4-ethylamino-6-isopropylamino-s-triazine) is a broad-spectrum herbicide used extensively for agricultural production and for farming activities around the world for the control of selective pre- and post-emergence weeds [1,2]. Atrazine studies have been focused on evaluating environmental and ecological toxicity because of the detection of environmentally relevant (0.1 µg/L), lethal and/or sub-lethal concentrations detected as chemical contaminants of rivers, streams and wells, which are common habitats for aquatic organisms and water sources for humans [3,4], and might constitute a public health problem.

Frogs, toads and the anuran group of amphibians are hugely responsive to ecological pollutants because of their semi-permeable skin and are thus suitable as bio-indicators for detecting the toxic effects of herbicides [5,6]. Over the last few decades, a global increase in endangered amphibian species has been reported [7], such as the *Xenopus laevis*, due to exposure to agrochemicals. The African clawed frog comes from the genus Xenopus, and they have a significant role in maintaining the water and terrestrial ecosystem where they can be both prey and predators, metamorphosing from an herbivorous tadpole to a carnivorous adult [8,9]. Although the *Xenopus laevis* has a lifespan of 15 years, there are some concerns as their population is threatened by water pollution.

The reported adverse effects of ATZ in anuran populations inhabiting agricultural sites and non-agricultural sites (with water bodies linked to herbicide use areas) include, amongst others, disruption of reproductive potential [10,11], histopathology changes [12–14], changes in oxidative stress parameters [15–17] and disruption of endocrine physiology [18,19]. However, the mechanisms of toxicity of atrazine and its attendant histopathology in metabolic organs such as the kidneys and liver are not yet fully understood.

Atrazine is widely believed to alter the production of adenosine triphosphate (ATP), thereby adjusting mitochondrial structure and impairing antioxidant defensive systems by causing oxidative damage in aquatic organisms through the formation of reactive oxidative species (ROS) [17,20]. This ROS-mediated damage is often indicated by biomarkers such as the levels of malondialdehyde (MDA) and lipid peroxidation levels (LPO) [21,22]. Additionally, LPO is known as a key step that modulates toxicities of a wide range of herbicides [15]. Furthermore, mitochondrial and oxidative damage culminates in necrosis and apoptosis by the release of pro-apoptotic proteins such as caspase-3 [23,24].

Atrazine-induced liver and kidney oxidative damage [15,17,25] and caspase-3 immunolocalization have been reported in other vertebrates and *Xenopus laevis* tadpoles, respectively, but reports on atrazine toxicities relative to hepato-renal surrogate markers such as AST, ALKp, ALT, blood urea nitrogen (BUN), creatinine (CREA) and the associated caspase-3 immuno-expression in the liver and kidney of post-metamorphic African clawed frogs (*Xenopus laevis*) are lacking. It is anticipated that atrazine-induced oxidative stress and caspase-3 toxicity observed in tadpoles and adult rats may be present in adult frogs. However, reports of atrazine-induced effects on hepatorenal biomarkers in juvenile and adult rats are inconclusive [25–27]. These conflicting reports between effects observed in tadpoles and rats indicate the differential effects of atrazine effects in both species (frogs and rats). Therefore, this study was designed against this backdrop to clearly delineate the hepatorenal histopathological impairment incurred by these environmentally sensitive adult frogs during atrazine use.

2. Materials and Methods

2.1. Chemical and Reagents

Atrazine obtained from Accu Standard Inc. (New Haven, CT, USA), 1, 1, 3, 3-tetraethoxypropane (TEP) and HPLC solvents (Sigma-Aldrich, Johannesburg, South Africa), KOH, KH2 PO4, perchloric acid (HClO4) and HPLC-grade water (Darmstadt, Germany) were used in this study. Kits for hepatic and renal function tests, alanine amino transferase (ALT), alkaline phosphate (ALKp) and aspartate amino transferase (AST) and renal creatinine (CREA) and blood urea nitrogen (BUN), were purchased from IDEXX Laboratories (Parktown, South Africa).

2.2. Preparation of Treatment Solutions for Selected Atrazine Concentrations

Twenty milligrams of 98.9% pure atrazine was used in preparing a standard stock solution of 4000 µg/L in dechlorinated tap water (pH 7.3). This stock was further diluted accordingly to obtain the concentrations: 0.01 µg/L, 200 µg/L and 500 µg/L of atrazine. Atrazine doses were chosen on earlier anuran reproductive toxicity study [28]. Thus, while 0.01 µg/L ATZ concentration resulted in disruptions of the endocrine system in frogs [29,30], 200 µg/L seemingly mimicked the effects reported in 0.01 µg/L ATZ concentration exposure [31], and 450 µg/L of ATZ and higher concentrations have also been used [28] as well. Though the highest dose of 500 µg/L or ppb of ATZ concentration used in the present study represents a midpoint between high and low dose points reported in literature for one to two weeks of exposure, this dose (500 µg/L or ppb) seems high enough to induce toxicity, if indeed ATZ is toxic, especially for sub-chronic exposure.

2.3. Animals and Housing

Forty (40) healthy, post-anuran metamorphosis male *Xenopus laevis* frogs used for this study were procured from African Xenopus Facility farm, Knysner, (Western Cape,

South Africa). The animals were randomly divided into four groups in four stainless steel tanks (225 cm × 24 cm × 12.5 cm) with water at the University of the Witwatersrand Animal Research Facility (UARF). They were allowed to acclimatize in tanks at UARF for 30 days prior to treatment, maintained a 12:12 h light/dark cycle, a room temperature of 22 ± 2 °C, oxygen saturation exceeding 70% and pH 6.5, according to methods of [32,33]. All experimental animal treatments were performed according to the ethical principles for animal research approved by the University Animal Research Ethics Committee (certificate number 2014/14/D) and Gauteng Nature Conservation (certificate 0115 and 0120).

2.4. Experimental Design and Procedure

The stainless-steel test aquaria were each filled with 60 L of water, according to the dose concentrations of ATZ and control group without ATZ. The frogs (40) were distributed at a density of 10 frogs per tank. The first tank contained zero ATZ concentration and the animals served as control, while the second, third and fourth tanks contained 0.01 µg/L, 200 µg/L and 500 µg/L ATZ concentrations, respectively, and housed the treated animals during the 3 months of sub-chronic exposure. Food, Kori TM Frog Brittle pellets (from Daro Pet Products, Johannesburg, South Africa) was provided ad libitum. Tank water was consistently aerated while recycling of the tank water occurred two times a week, to ensure a sterile environment throughout the length of the exposure/treatment. To regularly determine the atrazine concentration in each tank, once a week, 50 mL of water obtained from each tank was injected into a 200 mg Bond Elut Plexa solid phase extraction cartridge linked to gas chromatography–mass spectrometry (GC-MS, GC 6890, MS 5975, Agilent Technologies, CA, USA). Control tanks recorded zero atrazine, while treated groups maintained atrazine concentrations within the required levels in each tank as previously reported [32–34]. Thereafter, 0.02% benzocaine inhalation in a glass jar was used to anaesthetize the animals and blood was collected (through cardiac puncture) into specimen plain tubes and stored at room temperature and subsequently in the freezer (−80 °C) after clotting, pending laboratory analysis.

2.5. Lipid Peroxidation (LPO) Evaluation

The levels of oxidized lipids in vitro were marked by malondialdehyde (MDA) and were assessed with sensitive high-performance liquid chromatography (HPLC) in line with the method reported by Karatas et al. [35]. Samples were briefly analyzed with Bischoff HPLC device attached to a UV detector, collimated at 254 nm, and the analytical Prontosil column, Bischoff Chromatography (Leonberg, Germany) (12.5 cm × 4.0 mm, 5 µm particle size), was utilized for detection and measurement of MDA level. Sample injection volume was 50 µL, and flow rate was kept constant at 1 mL/min, while acetonitrile distilled water (50:50, *v*/*v*) was used for the mobile phase composition. MDA peaks were recorded relative to its retention time and established by spiking with added exogenous standard. MDA serum concentrations were calculated with the standard curve, prepared from 1, 1, 3, 3-tetraethoxypropane (TEP) and expressed as µg/mL.

2.6. Measurement of Serum Biochemical Markers

Appropriate kits were used to determine the levels of liver ALT, AST and ALKp, as well as urea and creatinine biomarkers of renal function, as set out by the manufacturers' procedures. Blood samples were centrifuged at 4000× *g* at 4 °C for 10 min, and obtained serum was subjected to spectrophotometric measurement of liver enzymes, ALT and AST, by the method of Reitman et al. [36]. Alkaline phosphatase (ALKp) was determined using an enzymatic colorimetric method as previously reported [37], while creatinine (CREA) and blood urea nitrogen (BUN) biomarkers were, respectively, determined according to methods previously described [38,39].

2.7. Samples Preparation for Histological Analysis

Liver and kidney fixed-tissue samples routinely processed overnight using automated tissue processor (Shandon Citadel 1000) were embedded in paraffin wax. Tissue blocks sectioned at 5 µm thickness using 2035 Biocut microtome (Leica, Germany) and sections stained with Mayer's haematoxylin and eosin and Van Gieson's stain were cover-slipped and analyzed for histo-morphological and connective tissue changes analysis, respectively.

2.8. Morphometry

Histological images were captured with a Leica ICC50 HD camera mounted to a light microscope (Leica DM500) linked to the Leica application suite (LAS EZ, version 3.0.0, Heerbrugg, Switzerland) imaging software through HP (intel) Xeon computer. Hepatocyte diameters were measured using the Fiji image analysis software [40] line width tool. Measurements of 20 hepatocytes per animal at ×100 magnification were restricted to only those with a visible nucleus and continuous outer lining. Only hepatocytes with visible nucleus and complete peripheral outline were measured at 100× magnification. Furthermore, the Fiji's image threshold plugin was used in measuring the percentage area of melanomacrophage at 10× magnification.

In the kidney, twenty photomicrographs per animal were used to measure corpuscle perimeter and epithelial cell height of both proximal convoluted and thick loop of Henle tubules, at 40× magnification. Tubules with a distinct lumen only were measured using Fiji's imaging software freehand tool. Connective tissue area fraction was measured by superimposing a grid (area per point = 500 pixels^2) in a single camera field (2048 × 1536 pixels^2) photomicrograph at 40× magnification and using the multi-point tool of Fiji image analysis software to count the number points that were stained for collagen. Eight randomly selected sections per group were analyzed and average counts were used for comparative analysis between groups.

2.9. Immunohistochemical Labelling of Caspase-3

Liver and kidney sections picked up on silane-coated slides were dewaxed, rehydrated and washed in 1 M phosphate buffer solution (PBS; pH 7.4) for 5 min. Thereafter, sections were incubated in 3% hydrogen peroxide in methanol for 30 min, washed three times in PBS and then incubated for one hour in 5% normal goat serum. After which, the sections were incubated overnight at 4 °C with anti-caspase-3 primary antibody (1:100 dilution, Ab 4059, Abcam). Tissue sections were washed three times in PBS and then (30 min room temperature) incubated with biotinylated goat anti-rabbit secondary antibody (1:1000 dilution, Vectastain, Vector Laboratories, Burlingame, CA, USA). Sections were washed three times in PBS followed by incubation in avidin–biotin complex (Vectastain ABC kit, Vector Laboratories, Burlingame, CA, USA) for 30 min. Sections were washed three times in PBS and then incubated with diaminobenzidine 3, 3′ tetrachloride (DAB) working solution for 5 min. Tissue sections were rinsed in running tap water, counterstained in haematoxylin, hydrated in alcohol, cleared in xylene and finally cover-slipped with Entellan new (Merck). The specificity of the anti-caspase-3 antibody was determined using tonsil tissue as the positive control. The negative control included omission of the primary antibody and substituting with PBS.

2.10. Statistical Analyses

Statistical analysis was carried out using Statistica TM (StatSoft) and Graph Pad prism software for Windows (version 7.0). All data were expressed as mean ± standard deviation (SD). One-way ANOVA was carried out, followed by post hoc Tukey's multiple comparison tests for statistical comparisons among the groups. The data obtained were presented in graphs with Microsoft Excel and Graph Pad prism software for Windows, respectively. Statistical significance was set at $p < 0.05$.

3. Results

3.1. Serum Levels of Liver, Kidneys Biomarkers and Lipid Peroxidation

In the 200 µg/L and 500 µg/L ATZ-treated groups, serum levels of ALT ($p < 0.0$ and $p < 0.01$, respectively) and creatinine ($p < 0.03$ and $p < 0.002$, respectively) were significantly increased in comparison to the control group (Figure 1A,D), with no significant difference ($p > 0.05$) in creatinine levels between the 200 µg/L and 500 µg/L treated groups. However, the levels of AST (Figure 1B), ALKp (Figure 1C) and BUN (Figure 1E) increased non-significantly ($p > 0.05$) in all the treated groups relative to the control group. The serum levels of MBA in the 500 µg/L ATZ-treated group significantly increased relative to the control group (Figure 1F).

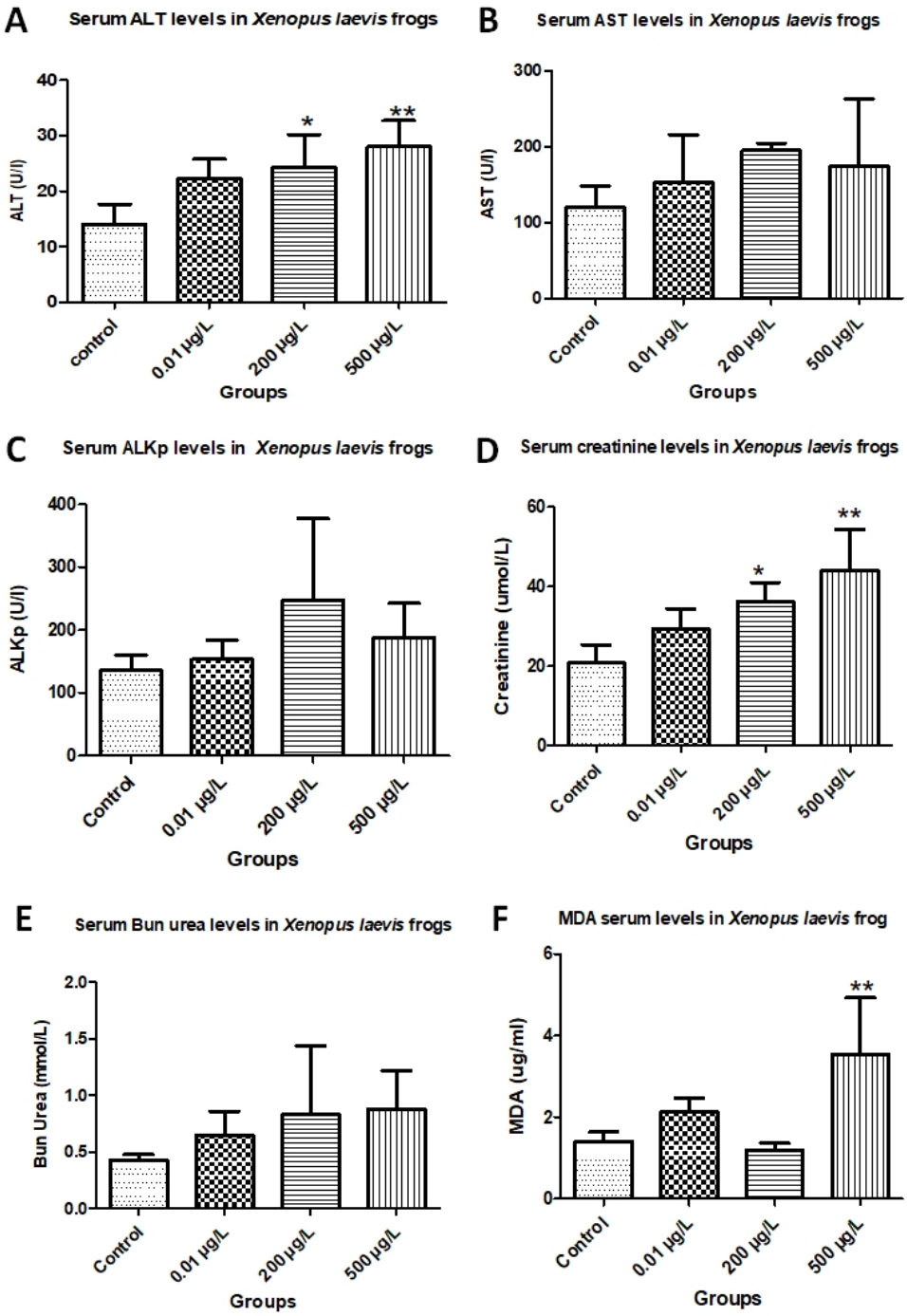

Figure 1. Effects of atrazine on serum levels of MDA, liver and kidney biomarkers in adult male *Xenopus laevis* frogs. (**A**) Serum ALT levels: * increased significantly in comparison to control $p < 0.05$;

** increased significantly compared to control $p < 0.01$. (**B**) Serum AST levels had no significant change between the control and treated groups. (**C**) Serum ALK_P levels had no significant change between the control and treated groups. (**D**) Serum creatinine levels: * increased significantly ($p < 0.05$) compared to control; ** significantly increased ($p < 0.01$) compared to control. (**E**) Serum BUN levels had no significant change between control and treated groups. (**F**) Serum MDA levels: ** significantly increased ($p < 0.01$) relative to control. Data represented as mean ± SD ($n = 10$). ALT: alanine aminotransferase; AST: aspartate aminotransferase; ALKp: alkaline phosphatase.

3.2. Histopathology

3.2.1. Liver Histopathology

The liver parenchyma revealed a normal microanatomy in the control group with radiating anastomosing cords of hepatocyte (arising from the central veins (Cv) (Figure 2A)) having one or two pale basophilic rounded nuclei and scanty cytoplasm (Figure 2I, red arrow). Between hepatic cords, narrow irregular hepatic sinusoids containing nucleated red blood cells were observed (Figure 2I, black arrow). At the portal triad, branches of the hepatic artery, hepatic portal vein and bile duct lined by simple cuboidal epithelium (Figure 2A, circled) and some melanomacrophages were observed (Figure 2A, red arrow).

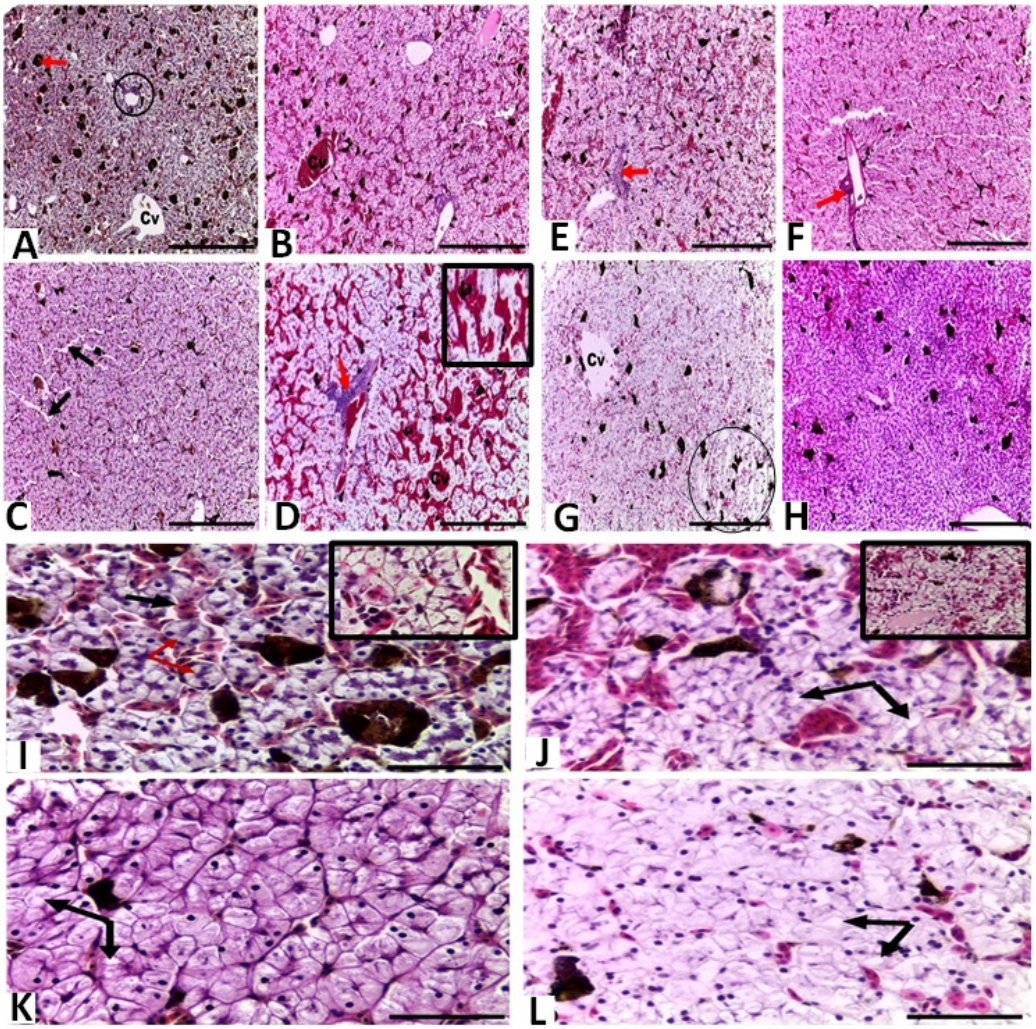

Figure 2. *Cont.*

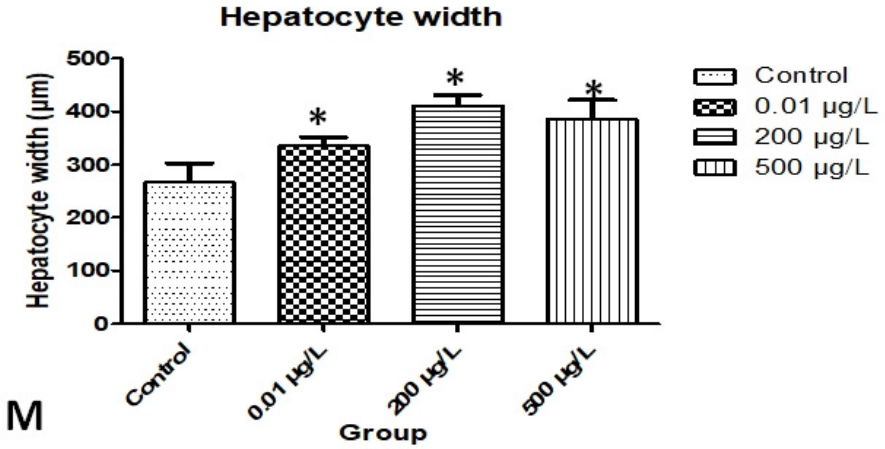

Figure 2. Photomicrographs of liver histopathology of frogs exposed to atrazine. (**A**) Control group with normal histology, central vein (Cv), portal triad (circle) and melanomacrophages (red arrow). (**B**) 0.01 µg/L group with clogged central vein (Cv). (**C**) 200 µg/L group with dilated sinusoids (black arrow). (**D**) 500 µg/L group with clogged central vein (Cv), sinusoidal congestion (insert) and portal inflammation (red arrow). (**E**) 0.01 µg/L group with portal inflammation (red arrow). (**F**) 200 µg/L group with portal inflammation (red arrow). (**G**) 500 µg/L group with parenchymal (circle) and central vein (Cv) necrosis. (**H**) 500 µg/L group with abundance of inflammatory cells. (**I**) Control group with normal hepatocyte histology (red arrow) alternating cords and sinusoid arrangement (insert) with nucleated red blood cells (black arrow). (**J**) 0.01 µg/L group with absence of normal hepatic cord arrangement (insert) and vacuolated hepatocytes (black arrow). (**K**) 200 µg/L group with highest observed hypertrophy with some vacuolation (black arrow). (**L**) 500 µg/L group with absence of hepatic cord arrangement and highly vacuolated hepatocytes (black arrows). (**M**) hepatocyte width with significantly increased * in comparison to control ($p = 0.003$). Values expressed as mean ± SD ($n = 10$). H&E stain. Scale bar in A to H = 240 µm (10× magnification). Scale bar in I to L = 38 µm (40× magnification).

In the atrazine-exposed groups, the 200 µg/L atrazine-exposed group revealed a dilated sinusoid (Figure 2C, black arrows), while in the 500 µg/L sinusoidal congestion with blood numerous haematopoietic cells were present (Figure 2D, insert), and infiltrating inflammatory cells were observed obscuring the liver tissues (Figure 2H). Parenchyma necrotic areas were observed in the 500 µg/L group (Figure 2C, circled), and portal inflammation was observed in all atrazine-exposed groups (Figure 2D–F). Hepatocyte cord disarrangement was observed in the 0.01 µg/L (Figure 2J) and 500 µg/L (Figure 2L) groups. Hepatocyte vacuolation was also observed in the 0.01 µg/L, 200 µg/L and 500 µg/L atrazine (Figure 2J–L, black arrows). Additionally, ATZ exposure of 200 µg/L and 500 µg/L significantly increased hepatocyte width ($p < 0.0003$) compared to the control (Figure 2).

Collagen tissue was increased in all the atrazine-treated groups periportally (Figure 3B–D: red arrows) and sinusoids (Figure 3F–H: red arrows) but not significantly increased relative to the control group (Figure 3I,J; $p > 0.050$). There was no collagen deposition observed within the hepatic lobules.

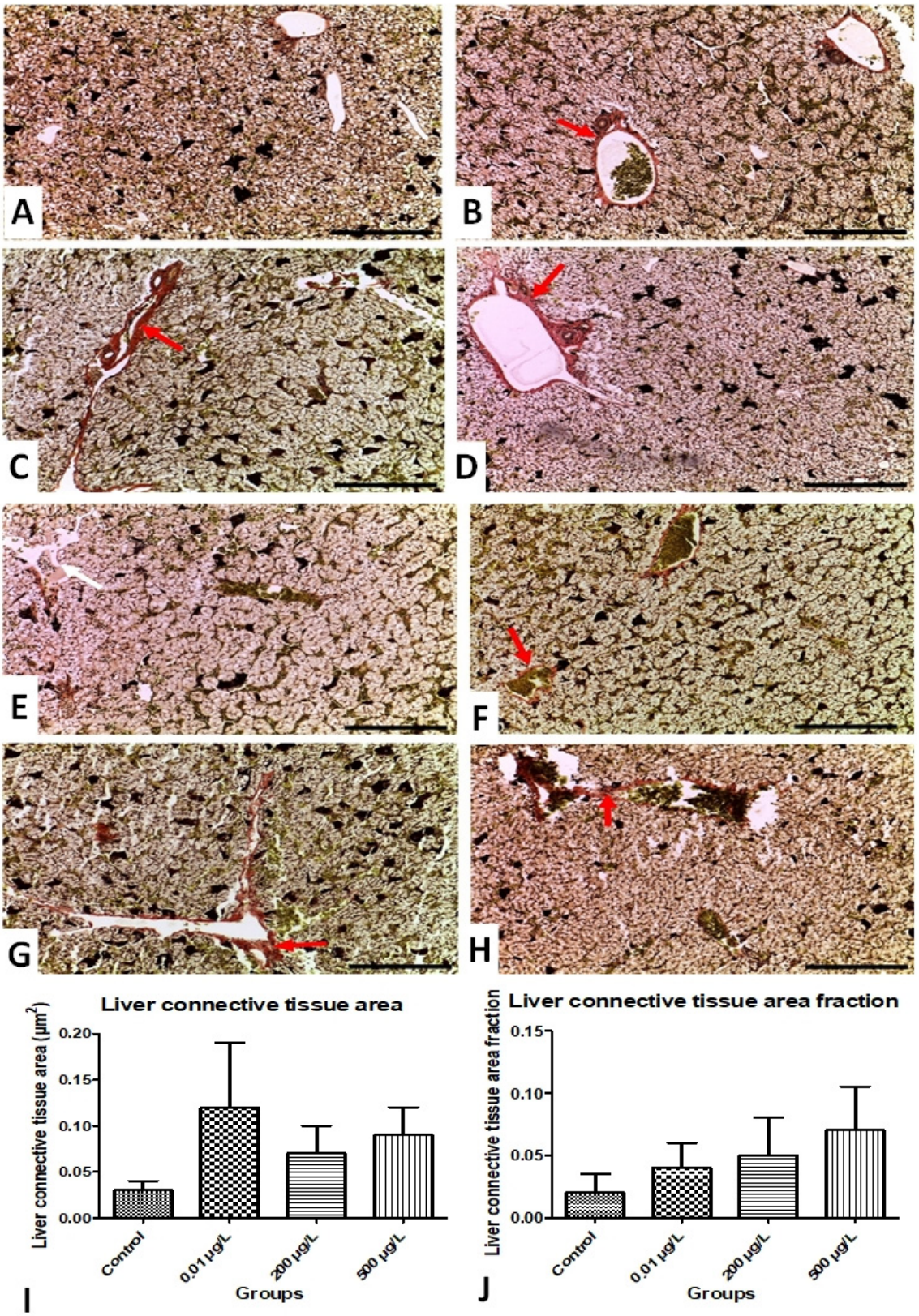

Figure 3. Photomicrographs of connective tissue profile in atrazine-exposed groups. (**A**) Normal connective tissue profile in control group. In (**B**–**D**), 0.01 µg/L, 200 µg/L and 500 µg/L groups, respectively, peri-portal fibrosis (red arrow). (**E**) Control group with normal connective tissue content and absence of peri-sinusoidal fibrosis. In (**F**–**H**), 0.01 µg/L, 200 µg/L and 500 µg/L groups, correspondingly, peri-sinusoidal fibrosis (red arrow). Van Gieson's stain, scale bar in A to D = 38 µm (40× magnification), scale bar in E to H = 38 µm (40× magnification). (**I**,**J**) No significant changes in liver connective tissue area and connective tissue area fraction.

3.2.2. Kidney Histopathology

The control group showed normal kidney histology, revealing normal proximal tubules (Figure 4A, black arrow), thick loop of Henle (Th) and distal tubules lined by simple short columnar and simple cuboidal epithelial cells, respectively (Figure 4A, red arrowhead). Collecting tubules with stratified cuboidal epithelial cells (white arrow) were observed. Hematopoietic cells were observed in the inter-tubular space with several red nucleated blood corpuscles (Figure 4A, red arrow). Vacuolized epithelial cells were noted within the tubules of the 0.01 µg/L group (Figure 4B, black arrow). In the 0.01 µg/L and 200 µg/L atrazine-exposed animals, tubular degeneration and loss of the epithelial cell–cell border of the thick loop of Henle were observed (Figure 4B,C, arrowhead). In the 500 µg/L group, the integrity of the thick loop of Henle tubule brush border was disrupted (Figure 4D, arrowhead).

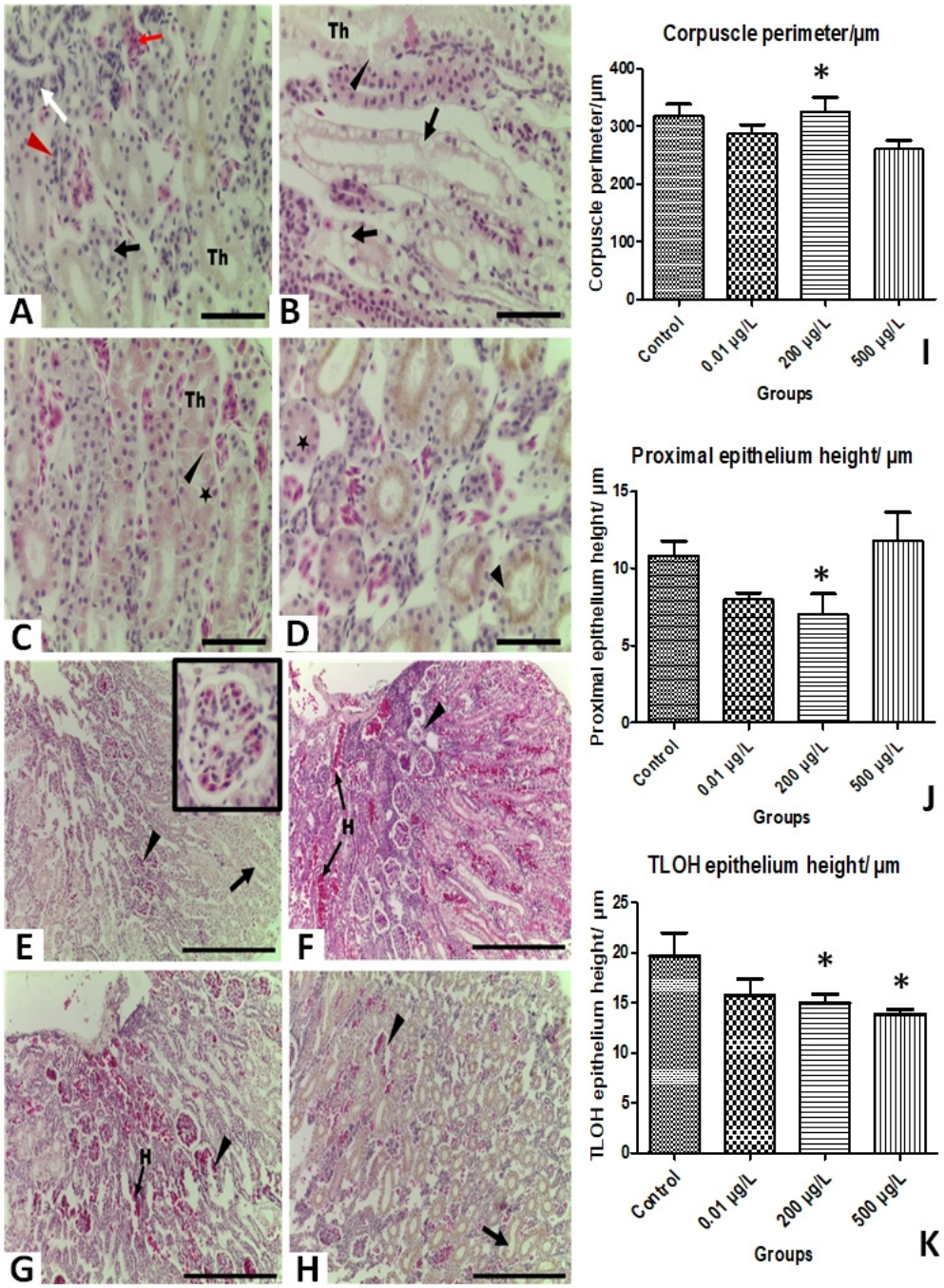

Figure 4. Representative photomicrographs of histopathologic findings in frog kidneys following

sub-chronic atrazine exposure. (**A**) Control with normal histology of proximal (black arrow), distal (red arrowhead), thick loop of Henle (Th) and collecting tubules (white arrow) and inter-tubular space with nucleated red blood cell (red arrow). (**B**) 0.01 µg/L group with degeneration of thick loop of Henle tubule (Th) and vacuolated tubules (black arrowhead). (**C**) 200 µg/L group with epithelial cell–cell boarder loss (black arrowhead) in thick loop of Henle, eosinophilic deposits (asterisk) inside the lumen of thick loop of Henle tubules (Th). (**D**) 500 µg/L group with loss of epithelial cell apical brush boarder (black arrowhead) and eosinophilic deposits (asterisk) in the proximal tubules. (**E**) Control with normal histology glomerulus (insert) and tubules (arrowhead). (**F**,**G**) 0.01 µg/L and 200 µg/L groups with glomeruli atrophy and necrosis (arrowhead) and peritubular hemorrhaging (**H**). (**H**) In 500 µg/L, mild glomerular atrophy (arrowhead) and dilated tubules (black arrow). (**I**–**K**) Corpuscle perimeter with proximal tubule epithelium height and thick loop of Henle epithelial height, respectively. * significantly decreased compared to control ($p < 0.05$; $p < 0.03$; $p < 0.01$, correspondingly). TLOH: thick loop of Henle. H&E stain, scale bar in A to D = 38 µm (40× magnification). Scale bar in E to G = 240 µm (10× magnification). Values are mean ± SD ($n = 10$).

The cortex of the control group showed normal renal corpuscles (Figure 4E, insert), but degeneration of the renal corpuscles, glomerular atrophy (Figure 4F–H, black arrowhead), dilation of tubular lumen in the 500 µg/L group (Figure 4H, black arrow) and vacuolized epithelial cells were noted within the tubule of the 200 µg/L group (Figure 4B, black arrow). Furthermore, there was shrinking of some tubules with eosinophilic material infiltration (Figure 4C,D, asterisk) and mild peritubular hemorrhaging (H) in the 0.01 µg/L and 200 µg/L groups (Figure 4F,G). The corpuscle perimeter and TLOH epithelial height were significantly reduced in the 500 µg/L group, while the proximal epithelium height and TLOH were significantly reduced in the 200 µg/L groups (Figure 4I–K). The 500 µg/L group significantly decreased in corpuscle perimeter compared to the control (Figure 4I, $p < 0.03$). The epithelium height of proximal tubules in the 200 µg/L group and thick loop of the Henle tubules in the 200 µg/L and 500 µg/L groups significantly decreased (Figure 4J,K, $p < 0.03$ and $p < 0.01$, correspondingly) relative to the control group.

3.2.3. Liver and Kidney Caspase-3 Immunohistochemistry

The expression of caspase-3 was predominantly in the epithelial and immune cells of the liver and not in the cytoplasm of hepatocytes. Controls showed no positive immunoreaction (Figures 5A and 6A). In the liver, caspase-3 expression was observed in Kupffer cells within the peri-sinusoidal space surrounding the hepatocytes (Figure 5B–D; red arrow) and in monocytes within the sinusoids (Figure 5B,D; black arrow) and sinusoidal endothelial cells (Figure 5B–D; blue arrowhead). Caspase expression was also observed in the bile duct epithelial cells of the 0.01 µg/L and 500 µg/L groups (Figure 5E,F, blue arrowhead). The number of melanomacrophages (MMCs) significantly decreased in the 0.01 µg/L and 500 µg/L groups ($p < 0.0001$) and in the 200 µg/L group ($p < 0.03$) compared with the control group (Figure 5G). In the kidney, caspase-3 expression was not observed in the control group (Figure 6A) but in the epithelial cells of cortical proximal tubules (Figure 6B,C,E; black arrow), distal tubule (Figure 6B,C,E; red arrow) and collecting tubules (Figure 6B,C,E white arrow) in all the atrazine-exposed groups instead. However, weak expression in the glomeruli was observed in the 0.01 µg/L group (Figure 6B,G). In the 200 µg/L (Figure 6D) and 500 µg/L (Figure 6E) groups, intensely expressed caspase-3 was observed in the podocytes (black arrowhead), simple squamous epithelial cells (white arrowhead) of the parietal layer and within the macula densa cells (circle) of the glomeruli.

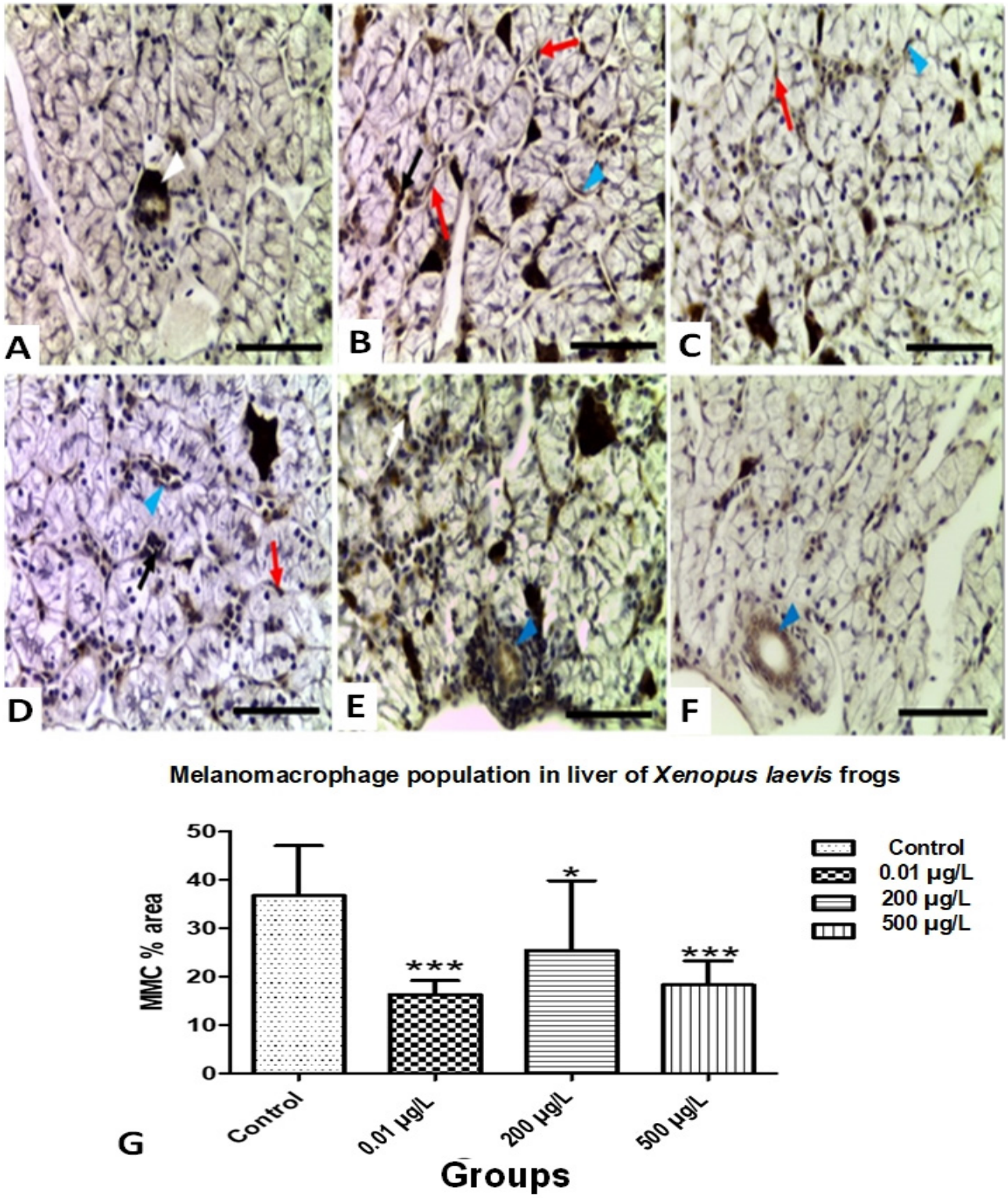

Figure 5. Expression of caspase-3 photomicrographs in *Xenopus laevis* liver cells with sub-chronic exposure to atrazine. (**A**) Liver tissue section showing melanomacrophages (white arrowhead) and lack of positive caspase-3 expression. (**B**) 0.01 µg/L, (**C**) 200 µg/L and (**D**) 500 µg/L) caspase-3 expression in monocytes in sinusoids (black arrow), Kupffer cells in the peri-sinusoidal space (red arrow) and flattened squamous endothelial cells lining sinusoids (blue arrowhead). (**E**,**F**) Caspase-3 expression in epithelial cells of bile ducts of the 0.01 µg/L and 500 µg/L groups, respectively. (**G**) The population percentage of melanomacrophages (MMC) in liver sections, * significantly decreased ($p < 0.05$) in comparison to control group; *** significantly decreased ($p < 0.001$) in comparison to the control group. Scale bar in A to F = 38 µm (40× magnification). Data presented as mean ± SD ($n = 10$).

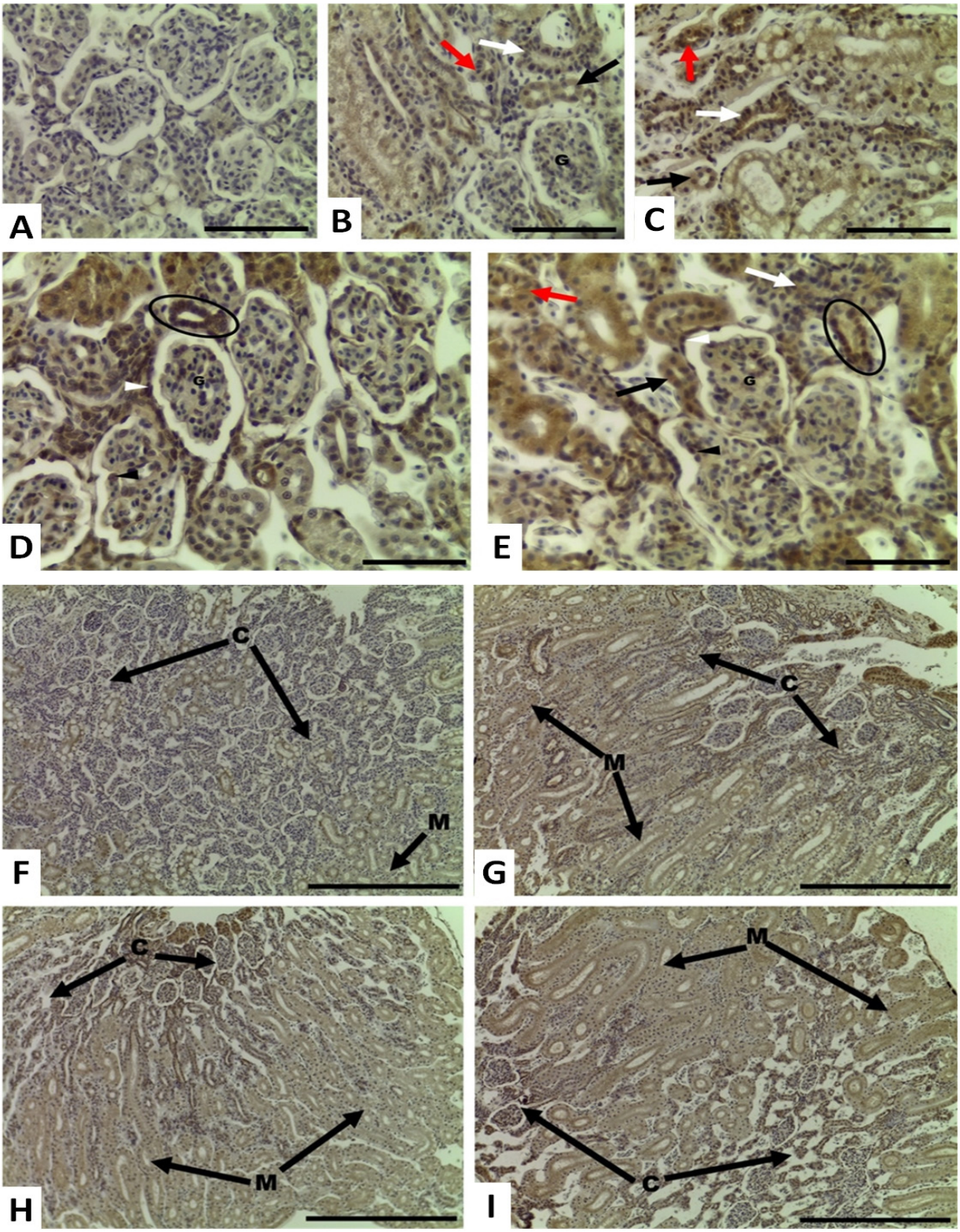

Figure 6. Photomicrographs of the expression of caspase-3 in frog kidneys following chronic exposure to atrazine. (**A**) Control with absence of caspase-3 expression. (**B**) 0.01 µg/L, (**C**) 200 µg/L and (**E**) 500 µg/L caspase-3 expression in epithelial cells of proximal tubules (black arrow), distal tubules (red arrow) and collecting tubules (white arrow). (**D**) 200 µg/L and (**E**) 500 µg/L caspase-3 expression in the glomeruli, macula densa cells (circle), podocytes (black arrowhead) and epithelial cells within the parietal layer (white arrowhead). (**F**) Control with low power absence of immuno-positive caspase-3 expression. (**G**) 0.01 µg/L, (**H**) 200 µg/L and (**I**) 500 µg/L caspase-3 expression in the cortex and medulla. Scale bar in A to E = 38 µm (40× magnification). Scale bar in F to I = 240 µm (10× magnification). C: cortex; M: medulla; G: glomerulus.

4. Discussion

The results have revealed the hepato-renal cytotoxicity of sub-chronic exposure to the pesticide atrazine in adult *Xenopus* frogs. Interestingly, the various doses of atrazine used showed variable significant levels of toxicity in the liver and kidneys, suggesting that, though this pesticide may be useful to increased agricultural productivity, caution must be applied in its application.

The significantly elevated serum MDA (500 μg/L exposed group) corroborates previous reports of elevated MDA in the liver, gills and muscles of bullfrog tadpoles [41] and in rats [25,42] exposed to atrazine. Correspondingly, the presence of hepatic cell injury with consequent functional implications is predicated on the significant increases in serum levels of ALT in the 200 μg/L and 500 μg/L exposure groups, as ALT levels function in the maintenance of cell membrane integrity [25,43]. However, the mildly reduced MDA level following 200 μg/L sub-chronic exposure suggests homeostatic adjustment adaptation in this group, as well as minimal adverse effects resulting from the non-significantly increased serum levels of AST and ALKp in all the treated groups, signifying the variable atrazine effects. This study utilized the sensitive high-performance liquid chromatography method, ensuring the accuracy of the measurements. The serum levels of ALT, AST and ALKp are markers of cell membrane integrity [26,43]. These results suggest hepatotoxicity and therefore disturbances of liver function following ATZ exposure.

Additionally, the assessment of renal function is based on the serum levels of urea and creatinine as biomarkers above or below the normal physiological level. Therefore, the non-significantly increased urea levels in all exposure groups and the significantly elevated creatinine levels in the 200 μg/L and 500 μ/L treated groups relative to the control group suggest renal glomeruli filtration dysfunction and/or impairment in all the treated groups but more severely in the 200 μg/L and 500 μ/L atrazine-exposed groups. The observed general trend in serum creatinine levels with a concentration-dependent effect in atrazine exposure suggests a greater adverse effect relative to urea as a renal biomarker.

Histopathology observations of hepatocyte perturbations are similar to reports observed in other atrazine-exposed species [44,45]. Atrazine-induced histological alteration is initiated by hypertrophy, as observed in the 200 μg/L and 500 μg/L exposed groups, as was previously reported [46] and which has been suggested to be an adaptive response to atrazine exposure [47]. Hepatocyte vacuolization observed in all our atrazine-exposed groups, particularly the 200 μg/L and 500 μg/L cohorts, has been reported in fish [45] and mice with attendant effects in lipid metabolism. Additionally, the observed central vein and sinusoidal congestion in the 0.01 μg/L and 500 μg/L groups suggest obstruction by immune cell migration and cellular breakdown debris. This corroborates with observations of vascular hemorrhaging indicated by erythrocyte infiltration into the hepatocytes reported in frogs exposed to 500 μg/L of ATZ. The red blood cell (erythrocytes) extravasation suggests compromised sinusoidal endothelium and may be a consequence of increased intra-sinusoidal pressure arising from vascular congestion [48]. Additionally, atrazine-induced perturbations in the immunology of amphibians are widely reported [49,50]. Similarly, the observed apoptosis of neutrophils and Kupffer cells confirmed by the expression of caspase-3 in the liver of atrazine-treated groups suggests the potential for atrazine to suppress phagocytic process or action and the gathering of monocytes directly or indirectly to sites of inflammation through induction of apoptosis in the immune cells. Contrastingly, a significant decrease in the population of MMCs observed in all the ATZ-exposed groups correlates with a field study report of aggregated melanomacrophages in the livers of *L. pipiens* exposed to atrazine [51]. Considering the role of MMCs in immunity (humoral and inflammatory responses) [52], the adult *Xenopus laevis* frogs' immunity may be adversely affected by different concentrations of atrazine.

The aforementioned histopathological changes seen in the kidneys of all the treated groups are similar to the effects reported following exposure to pollutants and pesticides [53,54]. Evidence of macula densa, podocyte and parietal cell (PECs) apoptosis is observed in the 200 μg/L and 500 μg/L atrazine-exposed groups. Apoptosis in podocytes is an indicator

of several kidney diseases [55], while parietal epithelial cell (PECs) apoptosis is speculated to serve as a means of regularizing glomerular cell number as reported by [56]. Therefore, the observed glomerular atrophy may be due to apoptosis of PECs and podocytes, and these cellular alterations may result in dysfunctions of glomerular filtration. Furthermore, apoptosis in the macula densa may lead to inhibition of auto-regulatory osmolarity reactions or processes. Together, glomeruli atrophy and macula densa apoptosis may explain the significantly increased levels of creatinine in frogs treated with high atrazine concentrations.

The significant reduction in tubular epithelium height and consequent dilation in the thick loop of Henle of the 500 µg/L atrazine-exposed group suggest a compromised regulation of extracellular fluid volume, urine concentration, calcium, magnesium, bicarbonate and ammonium homeostasis and urine protein composition [57]. Although caspase-3 was not expressed in the thick loop of Henle in the atrazine-exposed groups, caspase-3 was expressed in the proximal, distal and collecting tubule epithelial cells and increased with increasing atrazine concentrations, suggesting atrazine-induced apoptosis in the proximal and distal tubules but degeneration of the thick loop of Henle tubules, which may be induced by other mechanism such as activation of caspase-6 and 7 or extrinsic apoptotic pathways initiated by death receptors as reported by [58].

5. Conclusions

Atrazine-induced perturbations in the liver and kidney histomorphology and serum biomarker levels (ALT and creatinine) suggest severe hepatorenal toxicosis due to environmentally relevant atrazine concentrations. The observed hepatorenal histopathology cumulates in compromised metabolic, immunological and vascular function. Further associated pathophysiological effects associated with atrazine exposure at electron microscopic and molecular levels are required to elaborate on mechanisms through which these effects may impact the survival of frogs with continuous atrazine exposure. Thus, the constant presence of atrazine in the environment needs to be cautiously managed, as it remains a risk to the existence of *Xenopus laevis* frog populations and other animal species. Therefore, atrazine use, handling and disposal should be monitored and assessed regularly to prevent environmental health consequences on non-targeted aquatic species, especially amphibian biodiversity.

Author Contributions: Conceptualization, E.F.M., L.S. and J.A.J.; methodology, L.S., J.A.J. and E.F.M.; software, P.N., L.S. and J.A.J.; validation, E.F.M., L.S. and J.A.J.; formal analysis, L.S., J.A.J., E.F.M. and P.N.; investigation, L.S., J.A.J. and E.F.M.; resources, E.F.M., L.S. and J.A.J.; data curation, L.S., J.A.J., E.F.M. and P.N.; writing—original draft preparation, L.S. and J.A.J.; writing—review and editing, E.F.M., L.S., J.A.J. and E.F.M.; visualization, L.S., J.A.J. and E.F.M.; supervision, E.F.M.; project administration, E.F.M., L.S. and J.A.J.; funding acquisition, E.F.M., P.N., L.S. and J.A.J. All authors have read and agreed to the published version of the manuscript.

Funding: This work was supported by the University of Witwatersrand, Faculty of Health Science faculty research grant awarded to Lynette Sena.

Institutional Review Board Statement: The guidelines of the University of the Witwatersrand Animals Ethics Research Committee (2014/32/D) and the Gauteng Province Nature Conservation (CPF6 0115 (2015) and CPF6 0120, 2016) were followed in this study.

Informed Consent Statement: Not applicable.

Data Availability Statement: Data reported in this study will be made available on request, on acceptance of manuscript.

Acknowledgments: The authors specially acknowledge Hasiena Ali for her hands-on assistance at various stages of this research and Amadi Ihunwo, Luke Chimuka and Cornelius Rimayi for their amazing collaboration and inspiration.

Conflicts of Interest: The authors declare no conflict of interest.

References

1. Singh, A.; Kaur, C. Weed control with pre and post emergence herbicides application in spring planted sugarcane. *Sugar Tech.* **2004**, *6*, 93–94. [CrossRef]
2. Singh, A.; Virk, A.S.; Singh, J.; Singh, J. Comparison of pre- and post-emergence application of herbicides for the control of weeds in sugarcane. *Sugar Tech.* **2001**, *3*, 109–112. [CrossRef]
3. Mast, M.A.; Foreman, W.T.; Skaates, S.V. Current-use pesticides and organochlorine compounds in precipitation and lake sediment from two high-elevation national parks in the Western United States. *Arch. Environ. Contam. Toxicol.* **2007**, *52*, 294–305. [CrossRef] [PubMed]
4. Sousa, A.S.; Duaví, W.C.; Cavalcante, R.M.; Milhome, M.A.L.; do Nascimento, R.F. Estimated levels of environmental contamination and health risk assessment for herbicides and insecticides in surface water of Ceará, Brazil. *Bull. Environ. Contam. Toxicol.* **2016**, *96*, 90–95. [CrossRef] [PubMed]
5. Parmar, T.K.; Rawtani, D.; Agrawal, Y.K. Bioindicators: The natural indicator of environmental pollution. *Front. Life Sci.* **2016**, *9*, 110–118. [CrossRef]
6. Zaghloul, A.; Saber, M.; Gadow, S.; Awad, F. Biological indicators for pollution detection in terrestrial and aquatic ecosystems. *Bull. Natl. Res. Cent.* **2020**, *44*, 127. [CrossRef]
7. IUCN SSC Amphibian Specialist Group (IUCN). IUCN Red List of Threatened Species: *Xenopus laevis*. 2016. Available online: https://www.iucnredlist.org/en (accessed on 22 November 2021).
8. African Clawed Frog. *AZ Animals*. Available online: https://a-z-animals.com/animals/african-clawed-frog/ (accessed on 22 November 2021).
9. Garvey, N. *Xenopus laevis* (African Clawed Frog). *Animal Diversity Web*. Available online: https://animaldiversity.org/accounts/Xenopus_laevis/ (accessed on 22 November 2021).
10. Hayes, T.B.; Khoury, V.; Narayan, A.; Nazir, M.; Park, A.; Brown, T.; Adame, L.; Chan, E.; Buchholz, D.; Stueve, T.; et al. Atrazine induces complete feminization and chemical castration in male African clawed frogs (*Xenopus laevis*). *Proc. Natl. Acad. Sci. USA* **2010**, *107*, 4612–4617. [CrossRef]
11. Jooste, A.M.; Du Preez, L.H.; Carr, J.A.; Giesy, J.P.; Gross, T.S.; Kendall, R.J.; Smith, E.E.; Van Der Kraak, G.L.; Solomon, K.R. Gonadal development of larval male *Xenopus laevis* exposed to atrazine in outdoor microcosms. *Environ. Sci. Technol.* **2005**, *39*, 5255–5261. [CrossRef]
12. Coady, K.; Murphy, M.; Villeneuve, D.; Hecker, M.; Jones, P.; Carr, J.; Solomon, K.; Smith, E.; Van Der Kraak, G.; Kendall, R.; et al. Effects of atrazine on metamorphosis, growth, and gonadal development in the green frog (*Rana clamitans*). *J. Toxicol. Environ. Health* **2004**, *67*, 941–957. [CrossRef]
13. Murphy, M.; Hecker, M.; Coady, K.; Tompsett, A.; Jones, P.; Du Preez, L.; Everson, G.; Solomon, K.R.; Carr, J.; Smith, E.; et al. Atrazine concentrations, gonadal gross morphology and histology in ranid frogs collected in Michigan agricultural areas. *Aquat. Toxicol.* **2006**, *76*, 230–245. [CrossRef]
14. Papoulias, D.M.; Tillitt, D.E.; Talykina, M.G.; Whyte, J.J.; Richter, C.A. Atrazine reduces reproduction in Japanese medaka (*Oryzias latipes*). *Aquat. Toxicol.* **2014**, *154*, 230–239. [CrossRef]
15. Dornelles, M.F.; Oliveira, G.T. Effect of atrazine, glyphosate and quinclorac on biochemical parameters, lipid peroxidation and survival in bullfrog tadpoles (*Lithobates catesbeianus*). *Arch. Environ. Contam. Toxicol.* **2014**, *66*, 415–429. [CrossRef]
16. Gao, S.; Wang, Z.; Zhang, C.; Jia, L.; Zhang, Y. Oral Exposure to Atrazine Induces Oxidative Stress and Calcium Homeostasis Disruption in Spleen of Mice. *Oxidative Med. Cell. Longev.* **2016**, *2016*, 7978219. [CrossRef] [PubMed]
17. Semren, T.Ž.; Žunec, S.; Pizent, A. Oxidative stress in triazine pesticide toxicity: A review of the main biomarker findings. *Arch. Ind. Hyg. Toxicol.* **2018**, *69*, 109–125. [CrossRef]
18. Rohr, J.R. Atrazine and amphibians: Data re-analysis and a summary of the controversy. *bioRxiv* **2017**, 164673. [CrossRef]
19. Wirbisky, S.E.; Freeman, J.L. Atrazine Exposure and Reproductive Dysfunction through the Hypothalamus-Pituitary-Gonadal (HPG) Axis. *Toxics* **2015**, *3*, 414–450. [CrossRef]
20. Slaninova, A.; Smutna, M.; Modra, H.; Svobodova, Z. A review: Oxidative stress in fish induced by pesticides. *Neuroendocrinol. Lett.* **2009**, *30* (Suppl. 1), 2–12. [PubMed]
21. Lykkesfeldt, J. Malondialdehyde as biomarker of oxidative damage to lipids caused by smoking. *Clin. Chim. Acta* **2007**, *380*, 50–58. [CrossRef] [PubMed]
22. Grotto, D.; Maria, L.S.; Valentini, J.; Paniz, C.; Schmitt, G.; Garcia, S.; Pomblum, V.J.; da Rocha, J.B.T.; Farina, M. Importance of the lipid peroxidation biomarkers and methodological aspects FOR malondialdehyde quantification. *Química Nova* **2009**, *32*, 169–174. [CrossRef]
23. Redza-Dutordoir, M.; Averill-Bates, D.A. Activation of apoptosis signalling pathways by reactive oxygen species. *Biochim. Biophys. Acta* **2016**, *1863*, 2977–2992. [CrossRef]
24. Bayir, H.; Kagan, V.E. Bench-to-bedside review: Mitochondrial injury, oxidative stress and apoptosis—There is nothing more practical than a good theory. *Crit. Care* **2008**, *12*, 206. [CrossRef] [PubMed]
25. Liu, W.; Du, Y.; Liu, J.; Wang, H.; Sun, D.; Liang, D.; Zhao, L.; Shang, J. Effects of atrazine on the oxidative damage of kidney in Wister rats. *Int. J. Clin. Exp. Med.* **2014**, *7*, 3235–3243.
26. Jestadi, D.B.; Phaniendra, A.; Babji, U.; Srinu, T.; Shanmuganathan, B.; Periyasamy, L. Effects of Short Term Exposure of Atrazine on the Liver and Kidney of Normal and Diabetic Rats. *J. Toxicol.* **2014**, *2014*, e536759. [CrossRef] [PubMed]

27. Campos-Pereira, F.D.; Oliveira, C.A.; Pigoso, A.A.; Silva-Zacarin, E.C.; Barbieri, R.; Spatti, E.F.; Marin-Morales, M.A.; Severi-Aguiar, G.D. Early cytotoxic and genotoxic effects of atrazine on Wistar rat liver: A morphological, immunohistochemical, biochemical, and molecular study. *Ecotoxicol. Environ. Saf.* **2012**, *78*, 170–177. [CrossRef]
28. Freeman, J.L.; Rayburn, A.L. Developmental impact of atrazine on metamorphing *Xenopus laevis* as revealed by nuclear analysis and morphology. *Environ. Toxicol. Chem.* **2005**, *24*, 1648–1653. [CrossRef] [PubMed]
29. Kloas, W.; Lutz, I.; Urbatzka, R.; Springer, T.; Krueger, H.; Wolf, J.; Holden, L.; Hosmer, A. Does atrazine affect larval development and sexual differentiation of South African clawed frogs? *Ann. N. Y. Acad. Sci.* **2009**, *1163*, 437–440. [CrossRef] [PubMed]
30. Cooper, R.L.; Stoker, T.E.; Tyrey, L.; Goldman, J.M.; McElroy, W.K. Atrazine disrupts the hypothalamic control of pituitary-ovarian function. *Toxicol. Sci.* **2000**, *53*, 297–307. [CrossRef]
31. Zaya, R.M.; Amini, Z.; Whitaker, A.S.; Kohler, S.L.; Ide, C.F. Atrazine exposure affects growth, body condition and liver health in *Xenopus laevis* tadpoles. *Aquat. Toxicol.* **2011**, *104*, 243–253. [CrossRef] [PubMed]
32. Rimayi, C.; Odusanya, D.; Weiss, J.M.; de Boer, J.; Chimuka, L.; Mbajiorgu, F. Effects of environmentally relevant sub-chronic atrazine concentrations on African clawed frog (*Xenopus laevis*) survival, growth and male gonad development. *Aquat. Toxicol.* **2018**, *199*, 1–11. [CrossRef] [PubMed]
33. Asouzu Johnson, J.; Ihunwo, A.; Chimuka, L.; Mbajiorgu, E.F. Cardiotoxicity in African clawed frog (*Xenopus laevis*) sub-chronically exposed to environmentally relevant atrazine concentrations: Implications for species survival. *Aquat. Toxicol.* **2019**, *213*, 105218. [CrossRef]
34. Asouzu Johnson, J.; Nkomozepi, P.; Opute, P.; Felix, M. Cardiac and Cerebellar Histomorphology and Inositol 1,4,5-Trisphosphate (IP3R) Perturbations in Adult *Xenopus laevis* Following Atrazine Exposure. *Appl. Sci.* **2021**, *11*, 10006. [CrossRef]
35. Karatas, F.; Karatepe, M.; Baysar, A. Determination of free malondialdehyde in human serum by high-performance liquid chromatography. *Anal. Biochem.* **2002**, *311*, 76–79. [CrossRef]
36. Reitman, S.; Frankel, S. A colorimetric method for the determination of serum glutamic oxalacetic and glutamic pyruvic transaminases. *Am. J. Clin. Pathol.* **1957**, *28*, 56–63. [CrossRef] [PubMed]
37. Tietz, N.W.; Burtis, C.A.; Duncan, P.; Ervin, K.; Petitclerc, C.J.; Rinker, A.D.; Shuey, D.; Zygowicz, E.R. A reference method for measurement of alkaline phosphatase activity in human serum. *Clin Chem.* **1983**, *29*, 751–761. [CrossRef] [PubMed]
38. Larsen, K. Creatinine assay in the presence of protein with LKB 8600 Reaction Rate Analyser. *Clin. Chim. Acta* **1972**, *38*, 475–476. [CrossRef]
39. Coulombe, J.J.; Favreau, L. A New Simple Semimicro Method for Colorimetric Determination of Urea. *Clin. Chem.* **1963**, *9*, 102–108. [CrossRef]
40. Schindelin, J.; Arganda-Carreras, I.; Frise, E.; Kaynig, V.; Longair, M.; Pietzsch, T.; Preibisch, S.; Rueden, C.; Saalfeld, S.; Schmid, B.; et al. Fiji: An open-source platform for biological-image analysis. *Nat. Methods* **2012**, *9*, 676–682. [CrossRef] [PubMed]
41. Dornelles, M.F.; Oliveira, G.T. Toxicity of atrazine, glyphosate, and quinclorac in bullfrog tadpoles exposed to concentrations below legal limits. *Environ. Sci. Pollut. Res. Int.* **2016**, *23*, 1610–1620. [CrossRef]
42. Abarikwu, S.O. Protective Effect of Quercetin on Atrazine-Induced Oxidative Stress in the Liver, Kidney, Brain, and Heart of Adult Wistar Rats. *Toxicol. Int.* **2014**, *21*, 148–155. [CrossRef]
43. Soror, A.; Hozyen, H.; Eldebaky, H.; Soror, A.H.; Shalaby, H.M. Protective Role of Selenium Against Adverse Effects of Atrazine Toxicity in Male Rats: Biochemical, Histopathological and Molecular Changes. *Glob. Vet.* **2015**, *15*, 357–365. [CrossRef]
44. Wani, G.P.; Vibhandik, A.M. Effect of Atrazine (herbicide) on Histology and Protein Content of the Freshwater Teleost *Barbus carnaticus*. *J. Ecobiol.* **2011**, *29*, 257–265.
45. Mela, M.; Guiloski, I.; Doria, H.B.; Randi, M.; Ribeiro, C.O.; Pereira, L.; Maraschi, A.; Prodocimo, V.; Freire, C.; de Assis, H.S. Effects of the herbicide atrazine in neotropical catfish (*Rhamdia quelen*). *Ecotoxicol. Environ. Saf.* **2013**, *93*, 13–21. [CrossRef] [PubMed]
46. Ziegler, U.; Groscurth, P. Morphological features of cell death. *Physiology* **2004**, *19*, 124–128. [CrossRef] [PubMed]
47. Kaware, M. Changes in Liver and Body Weight of Mice Exposed to Toxicant. *Int. J. Sci. Eng.* **2013**, *3*, 92–95.
48. Kakar, S.; Kamath, P.S.; Burgart, L.J. Sinusoidal dilatation and congestion in liver biopsy: Is it always due to venous outflow impairment? *Arch. Pathol. Lab. Med.* **2004**, *128*, 901–904. [CrossRef]
49. Houck, A.; Sessions, S.K. Could Atrazine Affect the Immune System of the Frog, *Rana pipiens*? *Bios* **2006**, *77*, 107–112. [CrossRef]
50. Brodkin, M.A.; Madhoun, H.; Rameswaran, M.; Vatnick, I. Atrazine is an immune disruptor in adult northern leopard frogs (*Rana pipiens*). *Environ. Toxicol. Chem.* **2007**, *26*, 80–84. [CrossRef]
51. Rohr, J.R.; Schotthoefer, A.M.; Raffel, T.R.; Carrick, H.J.; Halstead, N.; Hoverman, J.; Johnson, C.; Johnson, L.B.; Lieske, C.; Piwoni, M.D.; et al. Agrochemicals increase trematode infections in a declining amphibian species. *Nature* **2008**, *455*, 1235–1239. [CrossRef] [PubMed]
52. Agius, C.; Roberts, R.J. Melano-macrophage centres and their role in fish pathology. *J. Fish Dis.* **2003**, *26*, 499–509. [CrossRef]
53. Khan, M.Z.; Yasmeen, G.; Parveen, S.; Akbar, A.; Zehra, A.; Hussain, B. Induced Effect of Permakil (Pyrethroid) and Sandaphos (Organophosphate) on Liver and Kidney Cells of *Euphlyctis cyanophlyctis*. *Can. J. Pure Appl. Sci.* **2010**, *5*, 1615.
54. Medina, M.F.; González, M.E.; Klyver, S.M.R.; Odstrcil, I.M.A. Histopathological and biochemical changes in the liver, kidney, and blood of amphibians intoxicated with cadmium. *Turk. J. Biol.* **2016**, *40*, 229–238. [CrossRef]
55. Matovinovic, M.S. 3. Podocyte injury in glomerular diseases. *EJIFCC* **2009**, *20*, 21–27. [PubMed]

56. Ohse, T.; Pippin, J.W.; Chang, A.M.; Krofft, R.D.; Miner, J.H.; Vaughan, M.R.; Shankland, S.J. The enigmatic parietal epithelial cell is finally getting noticed: A review. *Kidney Int.* **2009**, *76*, 1225–1238. [CrossRef] [PubMed]
57. Mount, D.B. Thick Ascending Limb of the Loop of Henle. *Clin. J. Am. Soc. Nephrol.* **2014**, *9*, 1974–1986. [CrossRef] [PubMed]
58. Alkhouri, N.; Carter-Kent, C.; Feldstein, A.E. Apoptosis in nonalcoholic fatty liver disease: Diagnostic and therapeutic implications. *Expert Rev. Gastroenterol. Hepatol.* **2011**, *5*, 201–212. [CrossRef]